Received: 5 April 2023 | Revised: 11 March 2024 | Accepted: 14 March 2024

DOI: 10.1111/mmi.15259

RESEARCH ARTICLE

WILEY

LC3B labeling of the parasitophorous vacuole membrane of *Plasmodium berghei* liver stage parasites depends on the V-ATPase and ATG16L1

Annina Bindschedler[1,2,3] | Jacqueline Schmuckli-Maurer[1] | Sophie Buchser[1] | Tara D. Fischer[4] | Rahel Wacker[1,3] | Tim Davalan[1] | Jessica Brunner[1] | Volker T. Heussler[1,2]

[1]Institute of Cell Biology, University of Bern, Bern, Switzerland

[2]Multidisciplinary Center for Infectious Diseases, University of Bern, Bern, Switzerland

[3]Graduate School for Cellular and Biomedical Sciences, University of Bern, Bern, Switzerland

[4]National Institute of Neurological Disorders and Stroke, National Institutes of Health, Bethesda, Maryland, USA

Correspondence
Volker T. Heussler, Institute of Cell Biology, University of Bern, Bern, Switzerland.
Email: volker.heussler@unibe.ch

Funding information
Schweizerischer Nationalfonds zur Förderung der Wissenschaftlichen Forschung, Grant/Award Number: 310030_182465; Intramural Research Program of the National Institute of Neurological Disorders and Stroke, Grant/Award Number: 1ZIANS003127-08; Multidisciplinary Center for Infectious Diseases (MCID), University of Bern, Switzerland, Grant/Award Number: MA-09

Abstract

The protozoan parasite *Plasmodium*, the causative agent of malaria, undergoes an obligatory stage of intra-hepatic development before initiating a blood-stage infection. Productive invasion of hepatocytes involves the formation of a parasitophorous vacuole (PV) generated by the invagination of the host cell plasma membrane. Surrounded by the PV membrane (PVM), the parasite undergoes extensive replication. During intracellular development in the hepatocyte, the parasites provoke the *Plasmodium*-associated autophagy-related (PAAR) response. This is characterized by a long-lasting association of the autophagy marker protein, and ATG8 family member, LC3B with the PVM. LC3B localization at the PVM does not follow the canonical autophagy pathway since upstream events specific to canonical autophagy are dispensable. Here, we describe that LC3B localization at the PVM of *Plasmodium* parasites requires the V-ATPase and its interaction with ATG16L1. The WD40 domain of ATG16L1 is crucial for its recruitment to the PVM. Thus, we provide new mechanistic insight into the previously described PAAR response targeting *Plasmodium* liver stage parasites.

KEYWORDS
autophagy, CASM, host-parasite interaction, liver stage, *Plasmodium*

1 | INTRODUCTION

Malaria remains one of the most devastating diseases with over 240 million estimated cases and still over 600,000 deaths per year (WHO, 2022). Its causative agent, the protist parasite *Plasmodium*, is injected into the human body by an infectious *Anopheles* mosquito during blood-feeding (Amino et al., 2006; Frischknecht et al., 2004). Before manifesting a symptomatic blood-stage infection, the parasite undergoes clinically silent replication in hepatocytes. Injected *Plasmodium* sporozoites migrate via the bloodstream to the liver sinusoids where they cross the endothelial barrier to enter the liver tissue (Pradel & Frevert, 2001; Tavares et al., 2013). They infect a hepatocyte by invagination of the host cell plasma membrane, leading to the formation of a

parasitophorous vacuole (PV) in which the parasite resides and develops throughout the liver stage development. Although the PV membrane (PVM) derives from the host cell plasma membrane, it is considerably remodeled by the parasite (Amino et al., 2008; Spielmann et al., 2012). Protein export to the PVM and maintenance of PVM integrity are critical for successful liver stage development. Once a productive liver stage infection is established, the parasite rounds up, transforms into a trophozoite, and eventually starts massive nuclear replication, resulting in a large multinuclear schizont. One liver schizont gives rise to thousands of daughter parasites, called merozoites. These merozoites are released into the host cell cytoplasm by PVM rupture which is followed by an ordered non-apoptotic host cell death. The merozoites are eventually transported into the bloodstream in host cell plasma membrane-derived vesicles termed merosomes (Sturm et al., 2006). Once merosomes rupture, they liberate merozoites, which invade red blood cells and thus initiate the erythrocytic infection cycle.

Host cells are equipped with a variety of mechanisms to eliminate intracellular pathogens. These cell defense mechanisms include autophagy and related responses (Agop-Nersesian et al., 2018; Levine et al., 2011; Romano et al., 2023). Autophagy is a catabolic process in the cell that allows the delivery of cytosolic material to lysosomal degradation (Morishita & Mizushima, 2019). Autophagosomes can form to recycle intracellular substrates in response to nutrient deprivation, or more selectively, autophagy can remove damaged or deleterious materials such as organelles and intracellular pathogens. Canonical autophagy is characterized by the de novo formation of double-membraned vesicles, termed autophagosomes, that sequester intracellular material and target it for degradation. This involves several multi-subunit protein complexes that drive the nucleation of a phagophore, its elongation, and closure into a double-membraned autophagosome that fuses with lysosomes in a final step (reviewed in Melia et al. (2020)). The nucleation of the phagophore is initiated by activation of the Unc51-like autophagy activating kinase (ULK) complex (ULK1/2, FIP200, ATG13, and ATG101) (Mizushima, 2010). The ULK complex further recruits and activates a class III phosphatidylinositol 3-kinase (PI3KC3) complex (Vps34, Beclin-1, ATG14, and Vps15) which leads to the generation of phosphatidylinositol 3-phosphate (PI3P) in the growing phagophore (Russell et al., 2013). PI3P attracts WD repeat domain phosphoinositide-interacting proteins (WIPIs). WIPI2 recruits ATG16L1, which is found in a complex with ATG5 and ATG12 to the phagophore to drive the conjugation of ATG8 proteins (LC3A/B/C and GABARAP/L1/L2) to phosphatidylethanolamine (PE) in an E3 ubiquitin-like manner, generating lipidated forms, such as LC3B-II, that are associated with autophagosomal membranes (Kabeya et al., 2000; Nakatogawa, 2013). Upon maturation and closure of the autophagosome, it fuses with lysosomes leading to the degradation of the cargo by soluble hydrolases within the lumen of the lysosome (Figure 1a). For the proper activity of these hydrolases, an acidic environment is required (reviewed in Yang & Klionsky (2010)). The proton gradient is established and maintained through the vacuolar-type H+-ATPase (V-ATPase) in the lysosomal membrane (Ohkuma et al., 1982).

In addition to canonical autophagy, during which ATG8 proteins are integrated into a de novo formed double-membrane, ATG8 proteins, including LC3B, can be conjugated to single-membrane, non-autophagosome compartments in processes summarized under the term CASM (conjugation of ATG8 proteins to single membranes) (Figure 1b). These processes that are associated with unconventional LC3 lipidation are commonly referred to as "non-canonical autophagy" (Durgan et al., 2021; Fletcher et al., 2018). Common to all non-canonical autophagy processes is that LC3B lipidation is independent of the nutritional status of the cell and upstream autophagy regulators such as the ULK complex (Florey et al., 2011; Martinez et al., 2015). Examples of CASM include LC3-associated phagocytosis (LAP), macropinocytosis (Florey & Overholtzer, 2012), entosis (Florey et al., 2011), LC3-associated endocytosis (Heckmann & Green, 2019), and cGAS-STING activation (Fischer et al., 2020). CASM has also been described to occur upon treatment with a range of drugs possessing lysosomotropic or ionophore properties, such as monensin and chloroquine (Florey et al., 2015; Hooper et al., 2022; Jacquin et al., 2017). LC3B lipidation to single-membrane perinuclear vesicles upon cGAS-STING activation depends on a mechanism called V-ATPase-ATG16L1-induced LC3B lipidation (VAIL) (Fischer et al., 2020). VAIL is independent of the ULK complex, WIPI proteins, and the PI3KC3 complex, but depends on the V-ATPase and its interaction with ATG16L1. Via ATG16L1 the conjugation systems needed for LC3B lipidation are recruited to the single membrane (Fischer et al., 2020). The V-ATPase and its interaction with ATG16L1 have recently been hypothesized to be the common denominator of all CASM pathways (Durgan & Florey, 2022).

We previously investigated autophagic targeting of *Plasmodium* parasites during the intracellular development in hepatocytes. We and others have shown that host cell autophagy-related processes influence the development of *Plasmodium* liver stages (Boonhok et al., 2016; Prado et al., 2015; Real et al., 2018; Thieleke-Matos et al., 2016; Wacker et al., 2017; Zhao et al., 2016). Autophagy-related processes acting as intracellular immune responses against liver stages are summarized under the term *Plasmodium*-Associated Autophagy-Related (PAAR) response (Agop-Nersesian et al., 2018). The PAAR response in hepatocytes infected with the rodent malaria parasite *Plasmodium berghei* is characterized by prolonged labeling of the PVM with LC3B (Grützke et al., 2014; Prado et al., 2015; Thieleke-Matos et al., 2016; Wacker et al., 2017). This LC3B labeling follows a non-canonical autophagy pathway, as it does not require key components of the autophagic machinery such as FIP200 of the ULK complex or the PI3KC3 complex (Figure 1c) (Bindschedler et al., 2021; Wacker et al., 2017). While about 30–50% of parasites are eliminated by this autophagy-related pathway, the other parasites can escape the host cell autophagic targeting and complete development into infectious merozoites (Prado et al., 2015).

Here, we focused on the molecular mechanism leading to LC3B localization at the PVM during the *Plasmodium* liver stage. We observed key players of VAIL and other CASM stimuli, such as

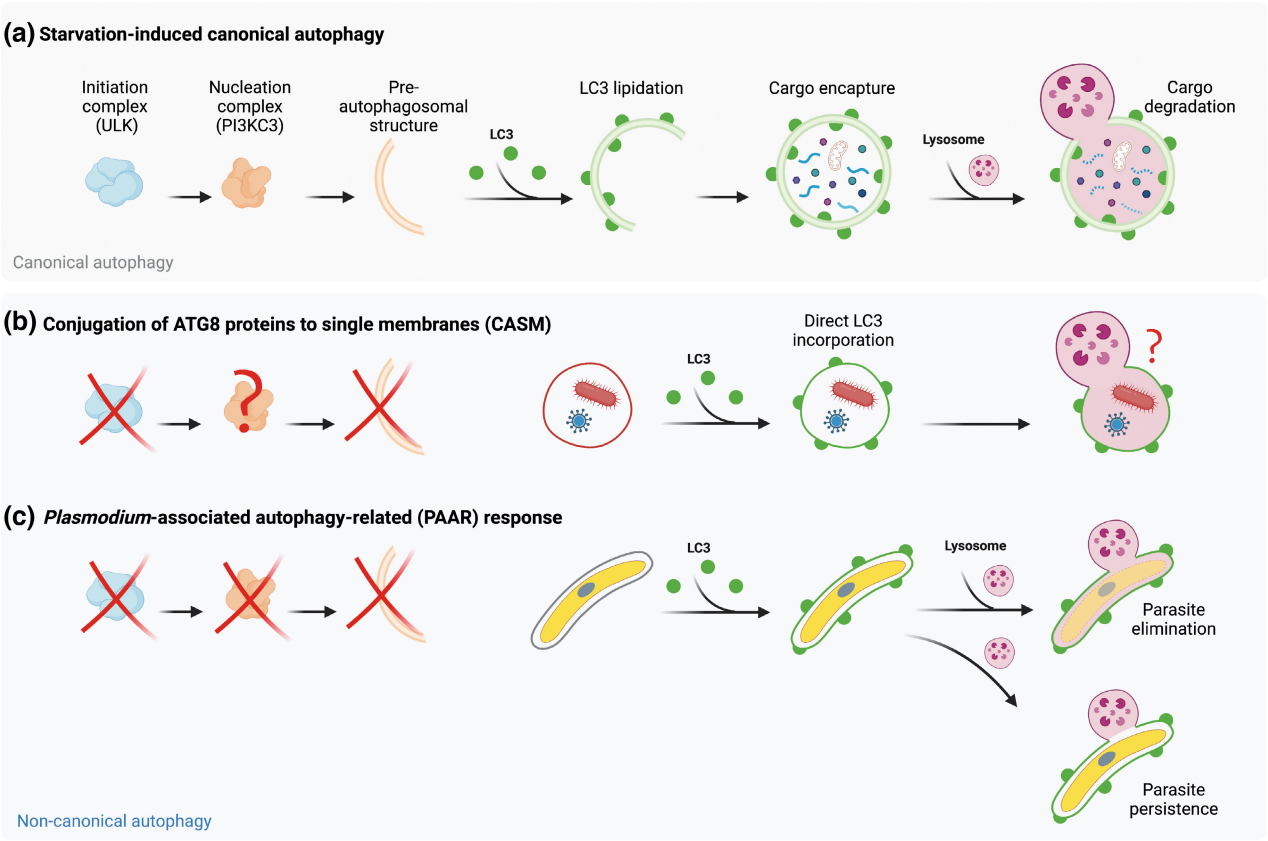

FIGURE 1 Canonical versus non-canonical autophagy pathways. (a) During starvation-induced canonical autophagy, a double-membraned autophagosome is formed around the randomly chosen substrate. Autophagosome formation involves the activity of the initiation complex ULK and the nucleation complex PI3KC3 and the LC3 lipidation machinery. Autophagosome cargo is degraded by fusion with lysosomes. (b) ATG8 proteins, such as LC3, can alternatively be conjugated to existing single membranes in a non-canonical autophagy process termed "conjugation of ATG8 proteins to single membranes" (CASM). This pathway is independent of the nutritional status of the cell and the upstream initiation complex ULK but dependent on the LC3 lipidation machinery. The term CASM includes a variety of molecular pathways, some of which involve the PI3KC3 complex, while others do not. (c) During the *Plasmodium* liver stage, LC3 is directly incorporated into the parasitophorous vacuole membrane (PVM) of the parasite, a process termed the *Plasmodium*-associated autophagy-related (PAAR) response. The PAAR response was shown to be independent of the ULK and PI3KC3 complexes and double-membrane formation, however, dependent on the core LC3 lipidation machinery. Lysosomes fuse with the PVM, however, this does not necessarily lead to parasite elimination. Schematic created with BioRender.com.

ATG16L1 and the host cell V-ATPase, at the PVM, and found them to be indispensable for LC3B localization at the PVM. Our work provides more mechanistic insight into the molecular pathway underlying autophagic host cell responses to *Plasmodium* parasites during the liver stage.

2 | RESULTS

2.1 | LC3B localization at the PVM is mediated by the WD40 domain of ATG16L1

To explore how LC3B localization at the PVM is induced independently of the ULK and PI3KC3 complexes, we examined the alternative VAIL pathway (Fischer et al., 2020). VAIL is mediated by direct recruitment of ATG16L1 to the V-ATPase, bypassing the need for upstream ULK complex initiation. ATG16L1 contains multiple protein domains and interaction motifs. The conserved N-terminal domain binds to ATG5 (ATG5-binding domain; ATG5-BD). This domain is followed by a coiled-coil domain (CCD), a central region allowing binding to FIP200 and WIPI2 (FIP200-binding domain; FBD), and a C-terminal WD40 domain (Dooley et al., 2014; Gammoh et al., 2013) (Figure 2a). Interestingly, while the WD40 repeats are crucial for interaction with the V-ATPase in VAIL, the WD40 domain has been consistently shown to be dispensable for recruitment of ATG16L1 during canonical autophagy (Fischer et al., 2020; Fletcher et al., 2018; Lystad et al., 2019; Xu et al., 2019). This renders ATG16L1 a genetic tool to dissect canonical or non-canonical autophagy pathways individually.

To investigate the role of ATG16L1 in LC3B recruitment to the PVM, we first analyzed its localization in *Plasmodium*-infected cells by using a cell line stably expressing BFP-ATG16L1. To visualize LC3B, cells were transiently transfected with GFP-LC3B. We observed a clear colocalization of ATG16L1 with LC3B at the PVM

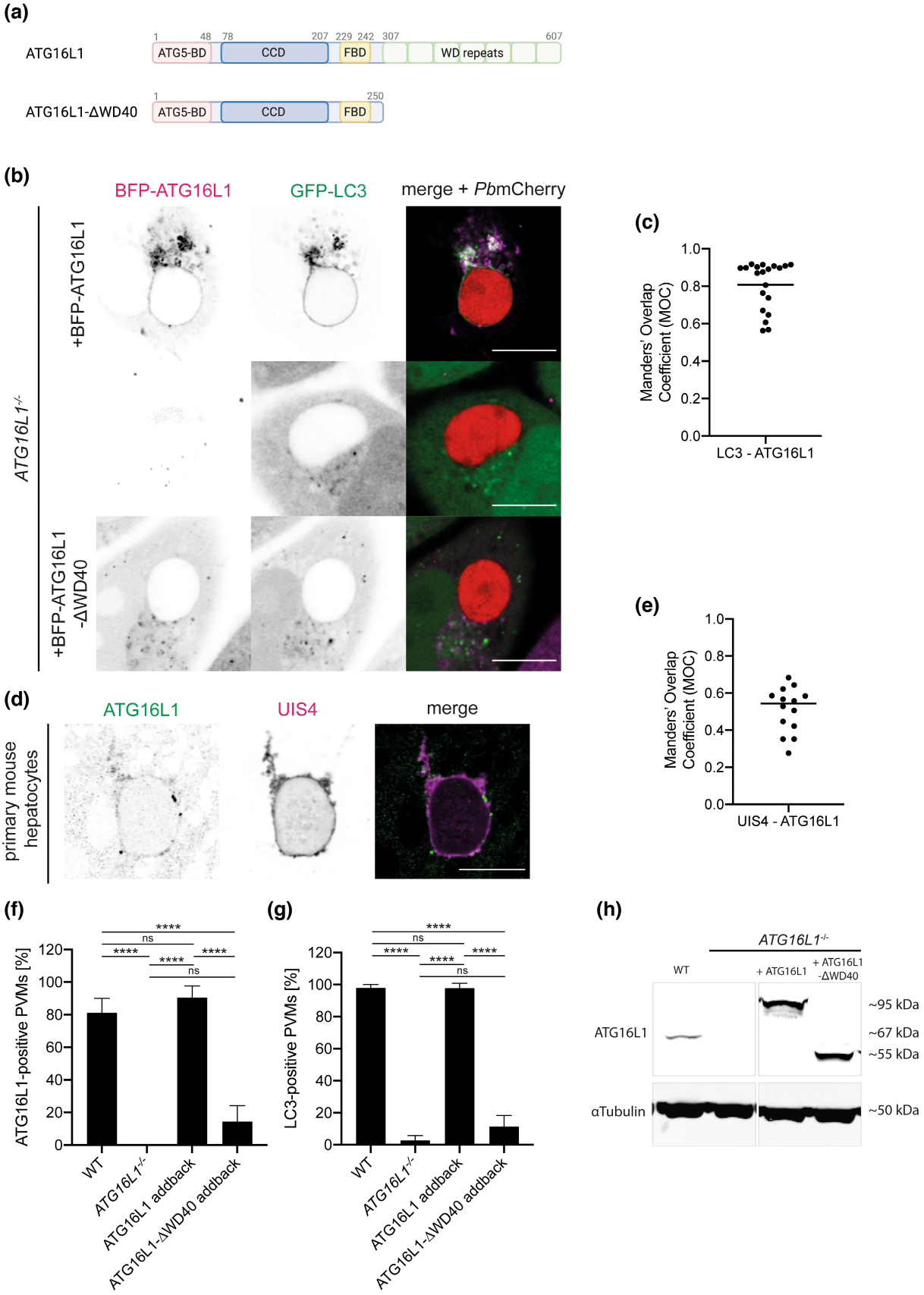

(Figure 2b,c). To further validate these results, we analyzed the localization of endogenous ATG16L1 by immunofluorescence assay (IFA) using an antibody directed against ATG16L1 and Upregulated in Infective Sporozoites 4 (UIS4), an exported PVM resident parasite protein and extended our investigation to additional cell types. In addition to HeLa cells (Figure S1A), we examined the

FIGURE 2 ATG16L1 recruits LC3B to the *Plasmodium berghei* PVM. (a) Schematic of the ATG16L1 protein structure. Human ATG16L1 is a 607 amino acid protein comprising four major domains: the N-terminal ATG5-binding domain (ATG5-BD; red), the coiled-coil domain (CCD; blue), a region encompassing binding sites for both FIP200 and WIPI2b known as FIP200-binding domain (FBD; yellow) and seven C-terminal WD40 repeats referred to as WD40 domain (green). The mutant used in the following experiments comprises amino acids 1 to 250 and excludes the WD40 domain. Schematic created with BioRender.com. (b) ATG16L1-deficient HeLa cells constitutively expressing BFP-ATG16L1 or BFP-ATG16L1-ΔWD40 (here in magenta) were transiently transfected with GFP-LC3B (green) and infected with *Pb*mCherry (red) parasites. At 24 hpi, cells were analyzed by live-cell confocal microscopy. Images were taken at a confocal laser scanning microscope and deconvolved using the Huygens Professional software. Scale bar: 10 μm. Note that the WD40 domain is required for ATG16L1 localization and LC3B localization at the PVM. (c) The graph shows the Mander's Overlap Coefficient (MOC) for BFP-ATG16L1 and GFP-LC3B. MOC was calculated using FIJI. $N = 20$ parasites. Each dot represents one parasite. (d) Primary mouse hepatocytes were infected with *Pb*mCherry parasites. At 24 hpi, cells were fixed and stained with anti-UIS4 (magenta) and anti-ATG16L1 antibodies (green). Images were taken with a confocal laser scanning microscope. Scale bar: 10 μm. (e) The graph shows the MOC for UIS4 and endogenous ATG16L1 in primary mouse hepatocytes. MOC was calculated using FIJI. $N = 14$ parasites. (f) Quantification of ATG16L1 localization at the PVM. HeLa WT, *ATG16L1*$^{-/-}$, *ATG16L1*$^{-/-}$ + BFP-ATG16L1, and *ATG16L1*$^{-/-}$ + BFP-ATG16L1-ΔWD40 cells were infected with *Pb*mCherry parasites. At 24 hpi, cells were fixed and stained with anti-ATG16L1 and anti-UIS4 antibodies to visualize the PVM. The percentage of UIS4-positive parasites showing ATG16L1 association with the PVM was determined in all four conditions. The graph depicts the mean and SD of three independent experiments. *P*-values were calculated using a one-way ANOVA test followed by Tukey's post hoc test (ns: $p > 0.05$; ****$p \leq 0.0001$). $N = 100$ per experiment and cell line. (g) Quantification of LC3B localization to the PVM. HeLa WT, *ATG16L1*$^{-/-}$, *ATG16L1*$^{-/-}$ + BFP-ATG16L1, and *ATG16L1*$^{-/-}$ + BFP-ATG16L1-ΔWD40 cells were infected with *Pb*mCherry parasites. At 24 hpi, cells were fixed and stained with anti-LC3 and anti-UIS4 antibodies to visualize the PVM. The percentage of UIS4-positive parasites showing a clear LC3B labeling of the PVM was determined in all four conditions. The graph depicts the mean and SD of three independent experiments. *P*-values were calculated using a one-way ANOVA test followed by Tukey's post hoc test (ns: $p > 0.05$; ****$p \leq 0.0001$). $N = 100$ per experiment and cell line. (h) Western blot of the cell lines used in (b). Whole protein lysates were separated on a 12% acrylamide gel, blotted onto a nitrocellulose membrane, and probed with an anti-ATG16L1 antibody. As a loading control, α-tubulin was detected.

localization of ATG16L1 in HuH7 cells, a hepatoma cell line frequently used in *Plasmodium* research (Figure S2A). Lastly, we investigated endogenous ATG16L1 localization in mouse primary hepatocytes, which represent a highly physiological system for studying *Plasmodium* infections (Figure 2d,e). In all the cell lines studied, including HeLa, HuH7, and mouse primary hepatocytes, we observed ATG16L1 localization at the PVM of *P. berghei* parasites, although with a lower degree of colocalization in primary hepatocytes. It is noteworthy that immunofluorescence analysis in primary hepatocytes posed challenges due to autofluorescence and enhanced background staining. Despite these obstacles, our findings consistently show ATG16L1's association with the PVM across various cell models.

At 24 h post infection (hpi), ATG16L1 and LC3B localized to the PVM in the majority of infected cells (Figure 2f,g). Importantly, LC3B recruitment to the PVM was completely abolished in *ATG16L1*$^{-/-}$ cells of HeLa as well as HuH7 background (Figure 2b,g; Figure S2B,D). Next, we examined the ability of full-length ATG16L1 and a truncated version of ATG16L1 lacking the WD40 domain (ATG16L1-ΔWD40; Figure 2a,h) to rescue LC3B association with the PVM in *ATG16L1*$^{-/-}$ HeLa cells. While reconstitution of *ATG16L1*$^{-/-}$ cells with the full-length ATG16L1 indeed rescued the original phenotype, reconstitution with ATG16L1-ΔWD40 failed to rescue LC3B positioning (Figure 2b,g; Figure S1A), indicating that indeed the WD40 domain is required for LC3B presence at the PVM. When analyzing the localization of the different ATG16L1 addbacks, we found full-length ATG16L1 at the PVM, while the ΔWD40 mutant did not (Figure 2b,f; Figure S1A) suggesting a direct interaction of ATG16L1 with the V-ATPase, similarly to VAIL. This, in turn, suggests that a V-ATPase must localize to the PVM.

2.2 | The V-ATPase recruits ATG16L1 to the PVM

Since we hypothesized that ATG16L1 is recruited to the PVM through the interaction of its WD40 domain with the V-ATPase, we next investigated the localization of the proton pump in infected cells.

We stably transfected cells with a GFP-tagged version of the V_1A subunit. As expected, a vesicular as well as cytosolic localization could be observed but importantly, GFP-V_1A also localized to the PVM of *Plasmodium* parasites, here visualized by expression of BFP-LC3B (Figure 3a,b). These results were further confirmed by making use of SidK, a bacterial effector protein deployed by *Legionella pneumophila*. SidK binds to the V_1A subunit of the V-ATPase to perturb V-ATPase function and delay acidification of the *Legionella*-containing vacuole (Abbas et al., 2020; Xu et al., 2010; Zhao et al., 2017). A truncated version of SidK, comprising amino acids 1–278, can be used as a tool to visualize the V_1A subunit of the V-ATPase (Maxson et al., 2022). We transiently transfected cells with $SidK_{1-278}$-GFP and analyzed its localization in *Plasmodium*-infected cells. Again, we found it localizing to vesicles, the PVM, and the tubovesicular network (TVN), an extension of the PVM (Figure 3c,d).

To examine the importance of the V-ATPase in ATG16L1 recruitment and LC3B localization at the PVM, we aimed to disrupt their association. The drug bafilomycin A1 (BafA1), a commonly used autophagy inhibitor, neutralizes lysosomal pH and blocks autophagosome–lysosome fusion (Yoshimori et al., 1991). After Baf1A treatment, the V_1A subunit of the V-ATPase was not observed at the PVM anymore (Figure S3A). Interestingly, we found that the addition of BafA1 completely blocked the LC3B labeling

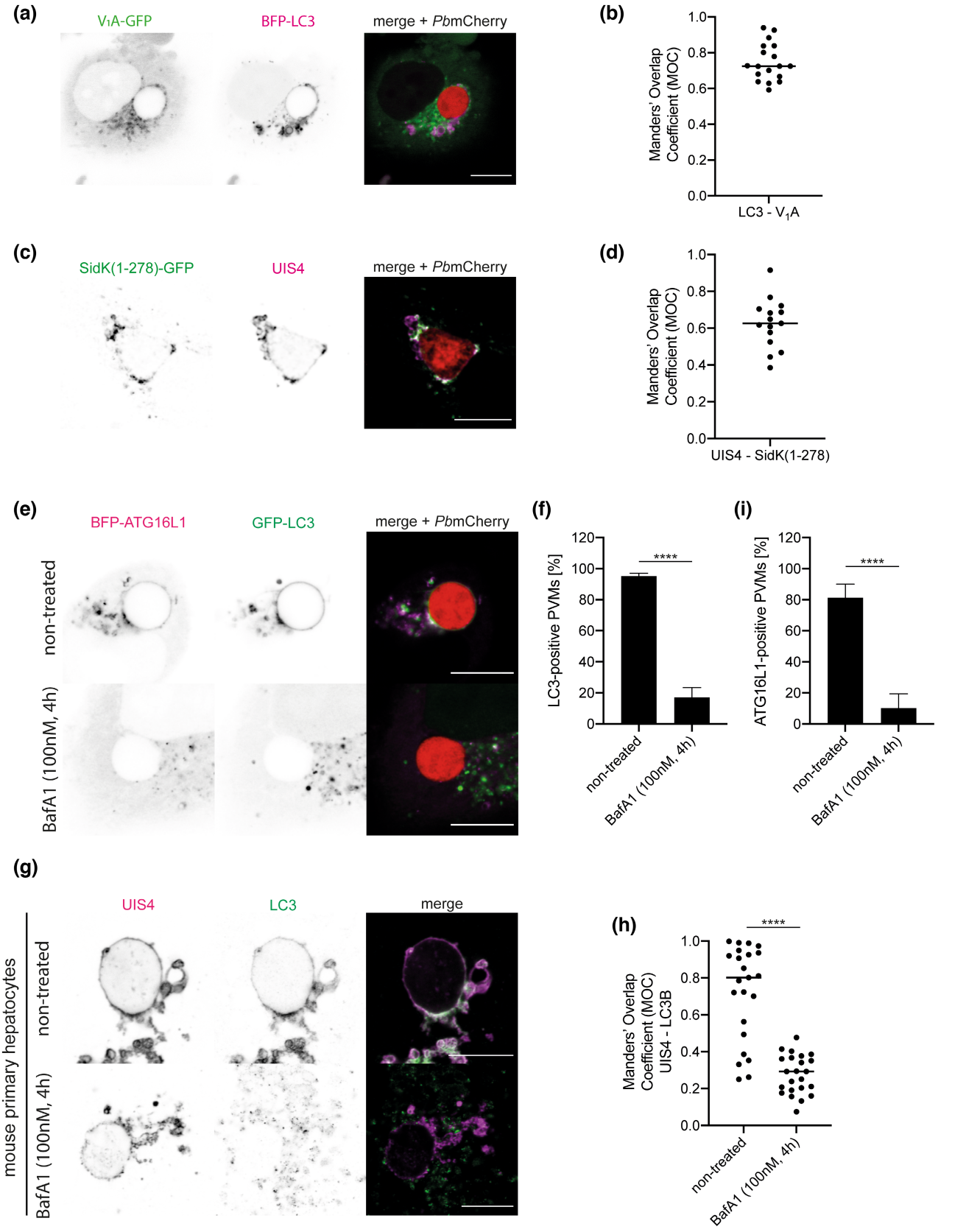

of the PVM in both HeLa cells and primary mouse hepatocytes (Figure 3e–h; Figure S1B). Furthermore, ATG16L1 localization to the PVM was also abolished after treatment with BafA1 (Figure 3e,i; Figure S1B), indicating that indeed the V-ATPase is important in attracting ATG16L1 and the associated LC3B lipidation machinery to the PVM.

FIGURE 3 The V-ATPase colocalizes with ATG16L1 at the PVM. (a) HeLa cells constitutively expressing V_1A-GFP (green) were transiently transfected with BFP-LC3B (magenta) to visualize the PVM and infected with *Pb*mCherry (red) parasites. Cells were analyzed by live-cell imaging at 24 hpi. Images were taken with a confocal laser scanning microscope. Scale bar: 10 μm. (b) The graph shows Mander's Overlap Coefficient (MOC) of BFP-LC3B and V_1A-GFP. The MOC was calculated using FIJI. Each dot represents one parasite. $N = 18$ parasites. (c) HeLa WT cells were transiently transfected with SidK(1–278)-GFP and infected with *Pb*mCherry parasites. At 24 hpi, cells were fixed and stained with anti-GFP (green) antibodies to enhance the GFP signal and anti-UIS4 (magenta) antiserum to visualize the PVM. Imaging was performed at a confocal laser scanning microscope. Scale bar: 10 μm. (d) MOC of UIS4 and SidK(1–278) is shown. Each dot represents one parasite. $N = 15$ parasites. (e) HeLa *ATG16L1*$^{-/-}$ + BFP-ATG16L1 (magenta) cells were transiently transfected with GFP-LC3B (green) and infected with *Pb*mCherry (red) sporozoites. At 20 hpi, cells were either left untreated or treated with 100 nM BafA1 for 4 h. Note that this 4-h treatment did not affect parasite viability. At 24 hpi, cells were analyzed by live-cell confocal microscopy. Scale bar: 10 μm. Note that BafA1 inhibits LC3B labeling of the PVM. (f) Quantification of LC3B-positive parasites in non-treated cells or cells treated with BafA1. HeLa cells stably expressing GFP-LC3B were infected with *Pb*mCherry and treated at 20 hpi with 100 nM BafA1 for 4 h. At 24 hpi, cells were fixed and the PVM was stained using anti-UIS4 antibodies. The percentage of UIS4-positive parasites that were also positive for LC3B was determined by microscopy. The graph depicts the mean and SD of three independent experiments. *P*-values were calculated using a Student's *t* test (****$p \leq 0.0001$). $N = 100$ per experiment and condition. (g) Mouse primary hepatocytes were infected with *Pb*mCherry parasites. 20 hpi, cells were either left untreated or treated with 100 nM BafA1 for 4 h. At 24 hpi, cells were fixed, stained with antibodies against UIS4 (magenta) and LC3B (green) and analyzed by confocal microscopy. Scale bar: 10 μm. (h) The graph shows the MOC of UIS4 and LC3B from the experiment described in (g). The MOC was calculated using FIJI. Each dot represents one parasite. $N = 23$ parasites per condition. (i) Quantification of ATG16L1-positive parasites in BafA1 treated cells. HeLa WT cells were infected with *Pb*mCherry sporozoites. At 20 hpi, cells were treated with 100 nM BafA1 for 4 h. Cells were fixed at 24 hpi and stained with anti-ATG16L1 and anti-UIS4 antibodies. The percentage of UIS4-positive parasites which showed ATG16L1 association was determined. The graph depicts the mean and SD of three independent experiments. *P*-values were calculated using a Student's *t* test (****$p \leq 0.0001$). $N = 100$ per experiment and condition.

2.3 | The bacterial effector protein SopF blocks LC3B labeling of the PVM

Although we very carefully controlled the BafA1 experiments and treated cells for 4 h only, drug treatments are still prone to artifacts as they can have negative effects on the parasite as well, which could then indirectly affect LC3B localization. In fact, BafA1 was shown to be a highly potent inhibitor of parasite growth with IC50s of only around 10–20 nM against *P. falciparum* blood stages of various strains (van Schalkwyk et al., 2010). As an alternative approach to tackling the host V-ATPase–ATG16L1 interaction, we, therefore, decided to use an inhibitor that can be exogenously expressed in the host cell. Recently, such an effector protein, SopF, has been discovered in *Salmonella typhimurium* and was shown to inhibit LC3B lipidation of the *Salmonella*-containing vacuole. SopF is secreted by *Salmonella* and acts by ADP-ribosylation of the c subunit in the V_0 complex of the V-ATPase, thereby inhibiting the interaction between the V-ATPase and the WD40 domain of ATG16L1. Importantly, SopF does not affect lysosomal pH or autophagosome–lysosome fusion. Therefore, SopF presents a valuable tool to inhibit VAIL without disrupting lysosomal function (Xu et al., 2019).

To investigate whether SopF abolishes LC3B labeling at the PVM of *Plasmodium* liver stage parasites, we generated HeLa cells stably expressing SopF-V5. Indeed, SopF expression, although leaving V_1A localization unaltered (Figure S3B), robustly inhibited LC3B and ATG16L1 recruitment to the PVM (Figure 4a–c; Figure S1C). Also, in the human hepatoma cell line HuH7, SopF expression led to the inhibition of LC3B labeling of the PVM (Figure S2C,D). These results corroborate our findings that BafA1 blocks LC3B localization at the PVM, further supporting the role of the V-ATPase in targeting the PVM of *Plasmodium* liver stage parasites.

Collectively, these results suggest that indeed the presence of and interaction between V-ATPase and ATG16L1 at the *Plasmodium* PVM is necessary for LC3B localization at the PVM.

2.4 | The VAIL trigger, cGAS-STING, is not required for LC3B localization at the PVM

Next, we wanted to know which signal triggers the observed recruitment of ATG16L1 to the PVM. Since the PAAR response in *P. berghei*-infected cells and the recently described VAIL mechanism share the molecular players to lipidate LC3B into single membranes, we first checked the main trigger of VAIL during LC3B lipidation into single-membrane perinuclear vesicles, stimulator of interferon response cGAMP interactor 1 (STING1) (Fischer et al., 2020). STING1 is a signaling molecule that is activated by the cyclic dinucleotide 2′3'-cGMP-AMP (cGAMP) that is synthesized by the DNA-sensing pattern recognition receptor cyclic GMP-AMP synthase (cGAS) upon detection of DNA (Ahn & Barber, 2019; Chen et al., 2016). It was described that cGAMP treatment of HeLa cells activates STING1 leading to LC3B lipidation onto single-membrane perinuclear vesicles through VAIL (Fischer et al., 2020; Gui et al., 2019). We were able to induce LC3B lipidation onto single-membrane perinuclear vesicles by cGAMP treatment only in WT cells and not in *STING1*$^{-/-}$ cells and thus achieved to reproduce data described in Fischer et al., 2020 (Figure S4A). We also observed STING1 translocation to these perinuclear vesicles upon cGAMP treatment as expected (Figure S4B). However, when we infected *STING1*$^{-/-}$ cells with *P. berghei* sporozoites and analyzed LC3B localization, LC3B localization at the *Plasmodium* PVM was not affected (Figure S4C). From this, we concluded that

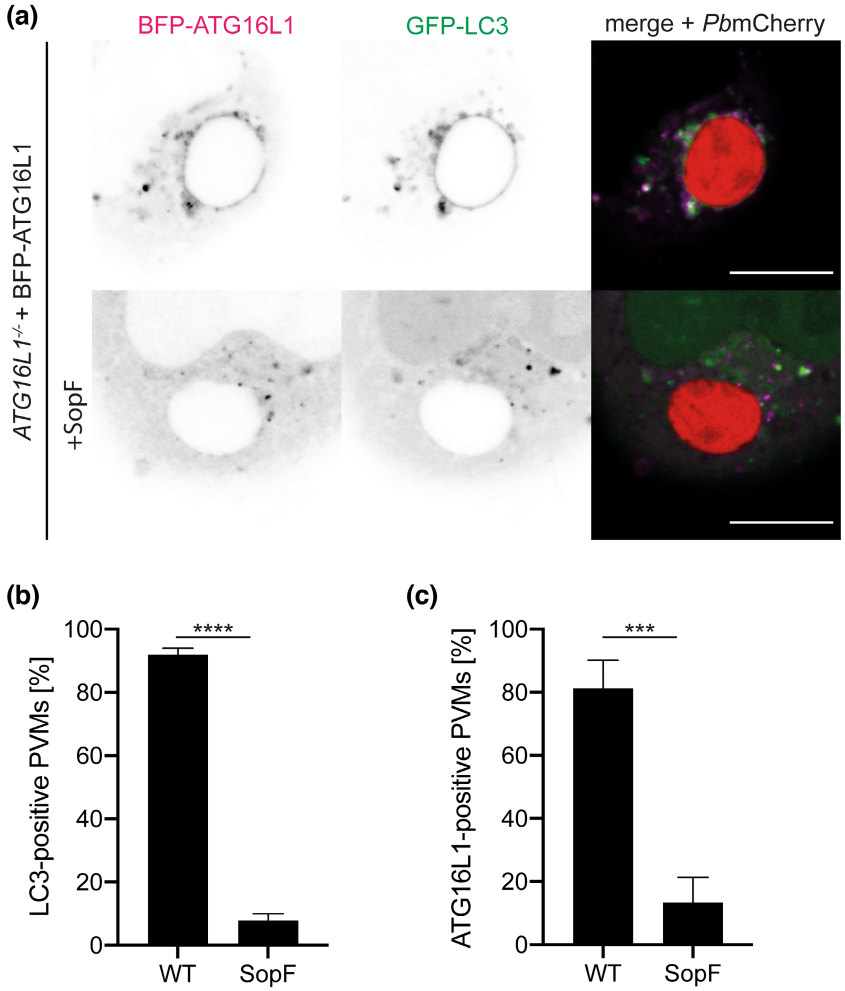

FIGURE 4 LC3B localization at the PVM is inhibited by the bacterial effector protein SopF. (a) ATG16L1-deficient HeLa cells constitutively expressing BFP-ATG16L1 cells were additionally stably transfected with a SopF-V5 expression plasmid. Control cells are only constitutively expressing BFP-ATG16L1 (magenta). Both cell lines were then transiently transfected with GFP-LC3B (green) and infected with *Pb*mCherry (red) parasites. At 24 hpi, cells were imaged by live-cell microscopy. Images were taken with a confocal laser scanning microscope. Scale bar: 10 μm. (b) Quantification of PVMs positive for LC3B in WT and SopF-expressing cells. HeLa WT and SopF-expressing cells were infected with *Pb*mCherry sporozoites. At 24 hpi, cells were fixed and stained with anti-LC3 and anti-UIS4 antibodies. The percentage of UIS4-positive parasites which were also positive for LC3B was determined by fluorescence microscopy. The graph depicts the mean and SD of three independent experiments. *P*-values were calculated using a Student's *t* test (***$p \leq 0.001$). $N = 100$ per experiment. (c) The percentage of PVMs positive for ATG16L1 was determined in HeLa WT and SopF-expressing cells by antibody staining of ATG16L1 and UIS4. The graph depicts the mean and SD of three independent experiments. *P*-values were calculated using a Student's *t* test (****$p \leq 0.0001$). $N = 100$ per experiment.

STING1 is not the trigger leading to LC3B localization at the PVM of *Plasmodium* liver stage parasites.

2.5 | The *Plasmodium* PVM contains phosphatidylserine

C-terminal lipidation of ATG8 represents a hallmark event during all autophagy-related processes. ATG8 lipidation was described earlier to occur exclusively to PE (Ichimura et al., 2000). However, a recent study provides evidence of alternative ATG8 lipidation to phosphatidylserine (PS) during CASM. In fact, ATG8 conjugation to PS was even suggested to be a molecular signature for CASM allowing its distinction from canonical autophagy (Durgan et al., 2021).

To confirm CASM as the main mechanism to conjugate LC3B to the PVM in *Plasmodium*-infected cells, we made use of a fluorescent sensor for PS, called Lact-C2 (Yeung et al., 2008). Lact-C2 was transiently expressed in HeLa cells, which were then infected with *P. berghei* sporozoites. Confocal microscopy indeed revealed GFP-tagged Lact-C2 at the PVM indicating that PS is enriched in the PVM (Figure S5A,B) colocalizing with LC3B (Figure S5C). This suggests that LC3B may indeed be conjugated to PS as well as to PE in the PVM. The functional relevance of this phenomenon, however, is not yet clear and needs further investigations that are beyond the scope of the current study. Still, this experiment provides a further hint

that CASM is the mechanism responsible for LC3B localization at the PVM.

2.6 | ATG16L1 deletion impacts parasite survival in HeLa cells

Finally, we wanted to know whether CASM at the PVM has any physiological relevance for parasite development. Both negative and positive effects have been correlated with LC3B localization to the PVM (Prado et al., 2015; Real et al., 2018; Thieleke-Matos et al., 2016; Wacker et al., 2017). A strong and prolonged LC3B labeling of the PVM has been shown to result in parasite elimination, but LC3B is also known to attract signaling molecules like p62, which can be beneficial for parasite survival (Bindschedler et al., 2022; Prado et al., 2015; Schmuckli-Maurer et al., 2017). The answer might be that the level of LC3B localization at the PVM at a given time makes the difference.

To evaluate the effect of completely blocking ATG8 lipidation, we analyzed parasite development in *ATG16L1*$^{-/-}$ HeLa and HuH7 cells by automated high throughput live-cell imaging and assessed parasite survival from 6 hpi to 48 hpi and parasite size at 48 hpi. Whereas parasite survival was reduced to less than 60% compared to parasites infecting WT HeLa cells (Figure 5a), the reduction in survival was less consistent in HuH7 cells (Figure S6A). Parasite size was not significantly affected by the knockout in HeLa and HuH7 cells (Figure 5b; Figure S6B; Figure S7C,D). We next performed

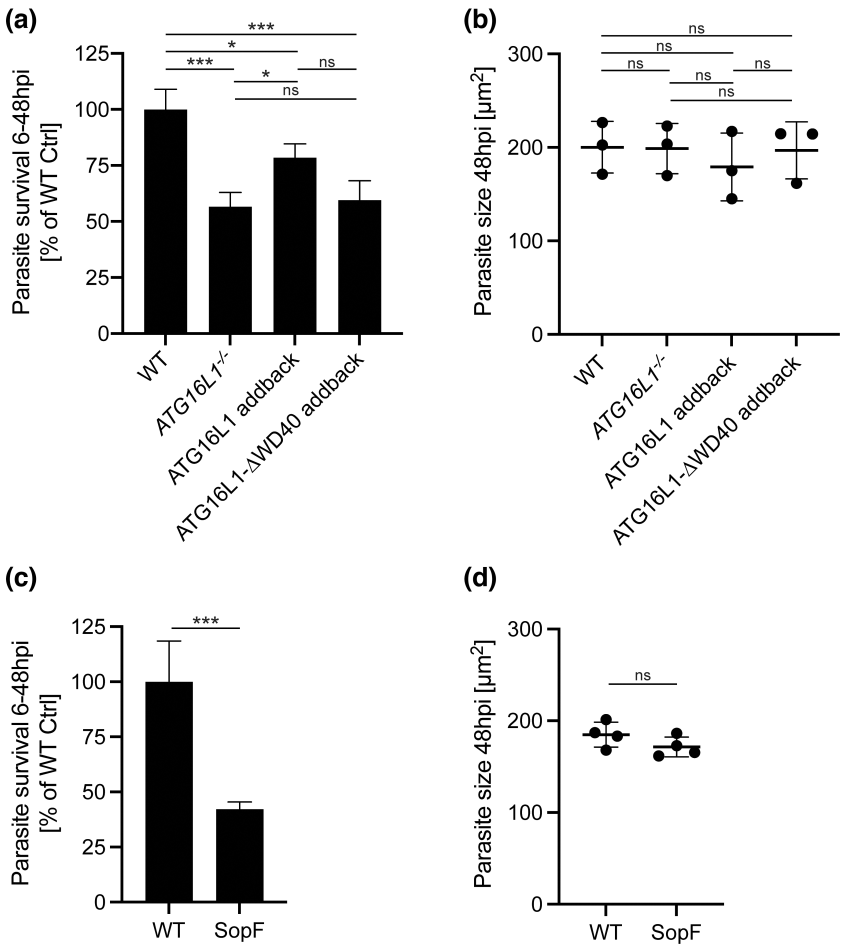

FIGURE 5 Parasite survival is reduced in cells deficient for non-canonical LC3B labeling of the PVM. (a) HeLa WT, *ATG16L1*$^{-/-}$, *ATG16L1*$^{-/-}$ + BFP-ATG16L1, and *ATG16L1*$^{-/-}$ + BFP-ATG16L1-ΔWD40 cells were infected with *Pb*mCherry. At 6 and 48 hpi, parasite numbers were evaluated using automated high throughput live-cell imaging and analysis (INCell Analyzer 2000). The graph shows relative parasite survival from 6 to 48 hpi compared to the WT control. The mean and SD of three independent experiments are depicted. $N > 500$ parasites per cell line and experiment. A one-way ANOVA test coupled with Tukey's post hoc test was used to determine *p*-values (ns: $p > 0.05$; $^{*}p \leq 0.05$; $^{***}p \leq 0.001$). (b) Parasite size at 48 hpi of the experiment described in (a). Each dot represents the median in parasite size of one experiment. The experiment was performed three times. Per experiment and cell line >250 parasites were analyzed. Mean and SD are depicted. *P*-values were calculated using a one-way ANOVA test followed by Tukey's post hoc test (ns: $p > 0.05$). (c) HeLa WT and SopF-expressing cells were infected with *Pb*mCherry. Parasite survival in the different cell lines was determined as in (a). The graph shows the relative survival compared to the WT control. The mean and SD of four independent experiments are shown. $N > 1500$ parasites per cell line and experiment. *P*-values were calculated using a Student's *t* test ($^{***}p \leq 0.001$). (d) Parasite size at 48 hpi of the experiment described in (c). Each dot represents the median in parasite size of one experiment. The experiment was performed four times. Per experiment and cell line >400 parasites were analyzed. Mean and SD are depicted. *P*-values were determined using a Student's *t* test (ns: $p > 0.05$).

reconstitution experiments to confirm that the observed phenotype was specific. Complementation with full-length ATG16L1 partly rescued the drop in survival rate in infected HeLa cells (Figure 5a), whereas complementation with ATG16L1 lacking the WD40 domain could not rescue the impaired survival rate (Figure 5a), indicating that the ATG16L1 WD40 domain, and therefore the missing non-canonical LC3B localization at the PVM, is responsible for the drop in parasite survival observed in HeLa cells.

To investigate this in further detail, we assessed parasite development in cells expressing the inhibitor of ATG16L1 association to the V-ATPase, SopF. Consistent with the results in the ATG16L1 mutants, we observed a drop in survival compared to parasites developing in WT HeLa cells (Figure 5c), while parasite size was not affected by the expression of SopF (Figure 5d; Figure S7D). Interestingly, parasites in all conditions analyzed seemed to develop normally until 24 hpi (Figure S7A,B). The decrease in survival mainly happens between 24 and 48 hpi, the time during which the parasite undergoes schizogony.

Our analysis suggests that ATG16L1, and potentially ATG8 family proteins, at the PVM may contribute to enhanced survival of *Plasmodium* parasites in WT HeLa cells. This observation is based on comparative survival rates in ATG16L1-deficient and WT HeLa cells, with reconstitution experiments indicating the importance of the ATG16L1 WD40 domain for this effect. While these findings imply a role for ATG8 lipidation at the PVM in parasite survival, they should be interpreted with caution due to the complexity of host–parasite interactions and the specific cellular context.

3 | DISCUSSION

Intracellular pathogens are exposed to cytosolic defense measures of the host cell. Vacuole-borne pathogens are often attacked and eliminated by the host cell through autophagy-related mechanisms. We showed earlier that during exoerythrocytic development, the PVM of *P. berghei* parasites is massively labeled with the autophagy marker protein LC3B (Prado et al., 2015). In this study, we provide novel insights into the molecular mechanism leading to this LC3B labeling.

Previous work identified that LC3B is localized to the already existing outer leaflet of the PVM and no additional double-membrane, as in canonical autophagy, is formed (Prado et al., 2015). LC3B localization at the PVM was shown to be independent of the ULK complex as well as the PI3KC3 complex but depends on the autophagy elongation machinery (Bindschedler et al., 2021; Wacker et al., 2017). In this study, we identified the V-ATPase and ATG16L1 as critical players in LC3B localization at the PVM. Our data suggest that the V-ATPase may play a role in facilitating the localization of ATG16L1, potentially through interactions involving the C-terminal WD40 domain of ATG16L1, at the PVM where LC3B localization occurs. These observations contribute to our understanding of the molecular mechanisms underlying LC3B association with the PVM, although the direct recruitment by the V-ATPase requires further validation (Figure 6).

Lately, alternative LC3B lipidation mechanisms have been described. During non-canonical autophagy, a subset of ATG proteins

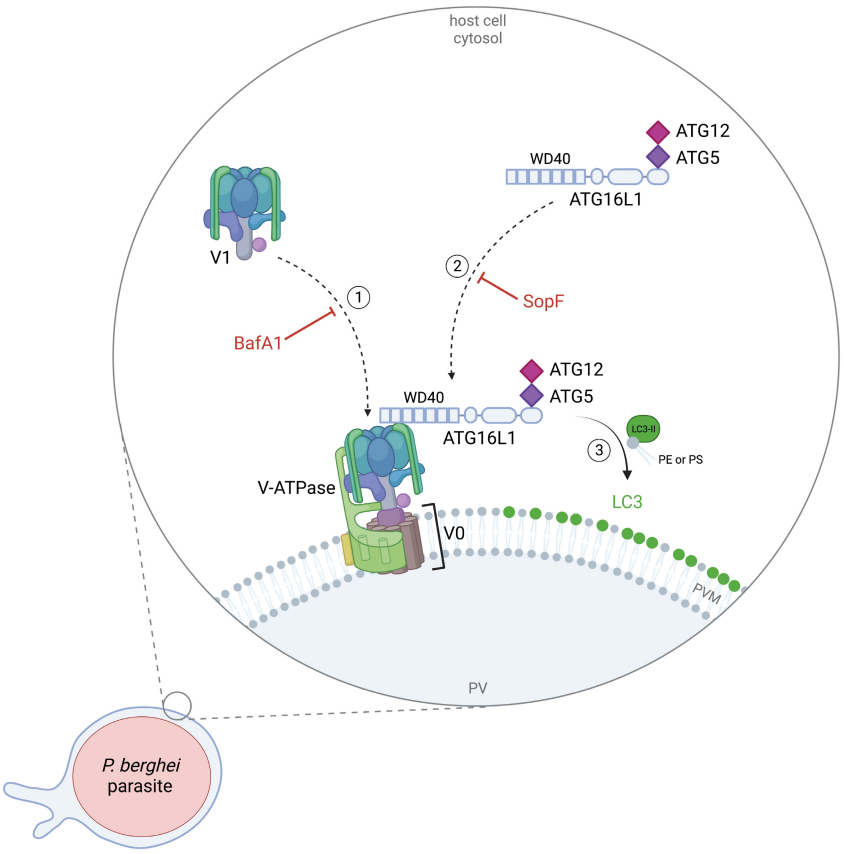

FIGURE 6 Schematic representation of the current hypothesis on how a molecular pathway could lead to LC3B labeling of the PVM of *Plasmodium berghei* liver stage parasites. ATG16L1 is recruited to the PVM by the V-ATPase. This interaction depends on the WD40 domain of ATG16L1. ATG16L1 recruitment is inhibited by the V-ATPase inhibitor Baf1A (1). The bacterial effector protein SopF impedes non-canonical LC3B localization to the PVM by inhibiting the interaction between the V-ATPase and ATG16L1 (2). LC3B is conjugated to PE or PS or both in the PVM of *P. berghei* liver stage parasites by the ATG16L1-ATG5-ATG12 complex (3). Schematic created with BioRender.com.

such as ATG3/5/7/12/16L1 target various single-membrane compartments for CASM in a mechanism independent of upstream autophagic regulators such as the ULK complex. Alternative lipidation of ATG8 proteins occurs during pharmacological CASM, LAP, *influenza A* infection, *Salmonella* infection, macropinocytosis, entosis, LC3-associated endocytosis, and cGAS-STING activation (Fischer et al., 2020; Fletcher et al., 2018; Florey et al., 2015; Florey et al., 2011; Heckmann & Green, 2019; Y. Xu et al., 2019). During cGAS-STING activation, STING1 translocates to single-membrane perinuclear vesicles to promote the assembly of the V-ATPase which in turn recruits ATG16L1 to promote LC3B lipidation (Fischer et al., 2020). Since the cGAS-STING pathway is a central cellular cytosolic double-stranded DNA sensor that allows cells to respond to infections (Burdette & Vance, 2013; Dhanwani et al., 2018) and it was recently published that *Plasmodium* DNA can be found in the hepatocyte cytoplasm upon infection (Marques-da-Silva et al., 2023), this pathway was hypothesized as the trigger for LC3B localization at the PVM upon *Plasmodium* infection. However, the fact that in *STING1*$^{-/-}$ cells normal LC3B lipidation can occur revealed that there must be alternative triggers in *P. berghei*-infected cells. Another pattern recognition receptor instead of STING1 may act to detect the intruder or the V-ATPase might itself detect infection by sensing perturbed ion gradients within the PV which influence the assembly or conformation of the pump.

The V-ATPase itself is a very versatile protein complex, involved in different cellular processes (Collins & Forgac, 2020). Interestingly, it is part of the nutrient-sensing machinery on the lysosomal membrane (Zhang et al., 2014; Zoncu et al., 2011). By recruiting the nutrient-sensing machinery to the PVM, parasites might potentially interfere with metabolic signaling. V-ATPase localization at the PVM also raises some exciting questions about its function as a proton pump. Despite its presence in the PVM (Figure 3a), most parasite-harboring vacuoles are not acidified (Niklaus et al., 2019). This may on one hand be because the PVM contains pores that allow diffusion of molecules up to 855 Da (Bano et al., 2007). On the other hand, the pH gradient might also be used by the parasite, for example, to support the symport of other molecules across the parasite membrane or even to generate ATP as it was reported that there are rotary ATPases in the parasite plasma membrane, and although not common for eukaryotes, they could potentially function in reverse acting as ATP synthases (Hayashi et al., 2000; Stewart et al., 2013). In summary, the V-ATPase function at the PVM raises very interesting hypotheses, which will be the focus of future investigations.

Interestingly, by expressing and secreting the effector protein SopF into the host cell cytosol, *Salmonella* bacteria evade LC3B labeling of the bacteria-containing vacuole by the host cell. *Salmonella*-containing vacuoles that cannot control vacuole labeling by LC3B are removed. Upon deletion of SopF in the bacterial genome, around 80% of all bacteria-containing vacuoles are labeled with LC3B and subsequently, the bacteria are eliminated (Y. Xu et al., 2019).

In *Plasmodium*, over 80% of all liver stage parasites are labeled with LC3B but many of them persist and successfully develop (Prado et al., 2015; Wacker et al., 2017). This suggests that *Plasmodium* has evolved different strategies to evade clearance by the autophagic machinery and potentially even benefits from it (Agop-Nersesian et al., 2018; Aguilera et al., 2024; Romano et al., 2023). Here, we even provide evidence that LC3B localization at the PVM supports parasite survival in infected HeLa cells. In HuH7 cells, this effect was not significant suggesting that the effect is cell-line dependent. This is not so surprising as transformed cell lines can compensate for the loss of effector molecules to different levels. Even a complete deletion of ATG16L1 in vivo might result in complementation effects as it also involves selection processes. A robust inducible degradation system could help to clarify the importance of LC3B labeling of the PVM but this was beyond the scope of this study. The focus of this study was to unravel the mechanism of LC3B labeling and for that ATG16L1-deficient HeLa and HuH7 cells are solid models.

It is noteworthy to consider that while we utilized LC3B as a specific readout, it is highly likely that all members of the ATG8 family undergo lipidation through the same mechanism. Consequently, in cells lacking ATG16L1 and SopF-expressing cells, conjugation of all these proteins to single membranes is supposed to be inhibited and they could potentially all contribute to the observed survival phenotype.

It was shown earlier that small parasites are covered with more LC3B, while bigger parasites exhibit less LC3B in their PVM suggesting that strong LC3B PVM labeling is deleterious for the parasite (Prado et al., 2015). There are mechanisms known that allow the parasite to regulate the amount of LC3B at the PVM, such as PVM shedding (Agop-Nersesian et al., 2017). Additionally, the activity of LC3B at the PVM seems to be regulated, as it was shown that the parasite PVM protein Upregulated in Infective Sporozoites 3 (UIS3) by interacting with LC3B protects the parasite from autophagic degradation (Real et al., 2018; Setua et al., 2020). However, we have shown here that completely blocking LC3B from localizing to the PVM also negatively influences parasite survival in HeLa cells, suggesting that there might be a threshold above which parasites are eliminated. Below this threshold, the parasite benefits from the presence of LC3B at the PVM. How can these, on the first view, puzzling findings be explained?

We previously published that parasite survival is positively supported by host cell signaling initiated by LC3B localization at the PVM. Through recruitment of p62 to the PVM by LC3B, the KEAP1-NRF2 pro-survival pathway is activated (Bindschedler et al., 2022). Interestingly, in the absence of the transcription factor NRF2, parasite survival is decreased to a similar extent as in SopF-expressing cells suggesting a link between non-canonical LC3B lipidation and NRF2 signaling. In support of this NRF2 survival signaling, a recent single-cell analysis of ex vivo *Plasmodium*-infected hepatocytes confirmed the upregulation of NRF2 target genes (Afriat et al., 2022).

C-terminal lipidation of ATG8 family proteins, including LC3B, represents a hallmark event during all autophagy-related processes. LC3B, while described earlier to be conjugated exclusively to PE during canonical autophagy (Ichimura et al., 2000), was recently found to undergo alternative lipidation to phosphatidylserine (PS) during CASM (Durgan et al., 2021). While classical autophagosomes

do not contain PS, we show that the PVM in fact contains PS (Figure S5). This suggests that LC3B may indeed be conjugated to PS as well as to PE in the PVM. Highly interesting in this context is that ATG8-PS has been proposed to be a longer-lived species compared to ATG8-PE, which might influence signaling dynamics (Durgan et al., 2021). This could indeed be a reason why the PVM is enriched in PS and contributes to prolonged LC3B labeling.

In this study, we delve into the mechanisms of LC3B labeling on the PVM during the *P. berghei* liver stage. Our research highlights the PAAR response as a subset of the CASM mechanism, closely following the pathways of VAIL and CASM. Notably, we present evidence suggesting the involvement of ATG16L1 in LC3B localization to the PVM, a crucial factor for regulating parasite survival within our HeLa cell in vitro model system. The applicability of these findings to in vivo scenarios remains to be explored in future studies.

Our results pave the way for a series of functional inquiries regarding the role of host cell ATG8 proteins throughout the development of the *Plasmodium* liver stage, particularly their contribution to pro-survival signaling within the host cell. This research opens new doors for understanding the intricate host–parasite interactions during *Plasmodium* liver stage development.

4 | EXPERIMENTAL PROCEDURES

4.1 | Animal work statement

Mice used in the experiments were between 6 and 12 weeks of age and were bred in the central animal facility of the University of Bern. Animal experiments were performed in strict accordance with the guidelines of the Swiss Tierschutzgesetz (TSchG; Animal Rights Laws) and approved by the ethical committee of the University of Bern (license number: BE86/19).

4.2 | Common parasite strains

All parasite strains used have a *P. berghei* ANKA background. *Pb*mCherry parasites are phenotypically wildtype (*Pb*WT) like. *Pb*mCherry parasites express cytosolic mCherry under the control of the *P. berghei* hsp70 regulatory sequences (Burda et al., 2015).

4.3 | Culture, treatment, and in vitro infection of HeLa and HuH7 cells and primary hepatocytes

HeLa cells (European Cell Culture Collection) and HuH7 cells (Japanese Collection of Research Bioresources Cell Bank JCRB0403) were cultured in Minimum Essential Medium with Earle's salts (MEM EBS; BioConcept, 1-31F01-I), supplemented with 10% FCS (GE Healthcare), 100 U penicillin, 100 µg/mL streptomycin, and 2 mM L-glutamine (all from Bioconcept). All cells were cultured at 37°C and 5% CO_2 and split using accutase (Innovative Cell Technologies). For inhibitor treatments, cells were incubated in media containing 100 nM bafilomycin A1 (Merck B1793) for 4 h.

Primary murine hepatocytes were isolated as described elsewhere (Prado et al., 2015) and cultured in William's E medium (Bioconcept 1-48F02-I) supplemented with 10% FCS (GE Healthcare), 100 U penicillin, 100 µg/mL streptomycin, and 2 mM L-glutamine (all from Bioconcept) at 37°C and 5% CO_2.

For infection of cells, the salivary glands of infected *Anopheles stephensi* mosquitoes were isolated and disrupted to release sporozoites. Sporozoites were incubated with cells in the normal growth medium.

4.4 | Plasmids and generation of stable cell lines

The plasmid encoding GFP-LC3B was kindly supplied by Prof. Johji Inazawa (Tokyo Medical and Dental University, Japan). The pEBFP2-LC3B plasmid was generated as described previously (Niklaus et al., 2019). The plasmid encoding EGFP-Lact-C2 was a gift from Sergio Grinstein (Addgene plasmid #22852) (Yeung et al., 2008). The plasmid encoding SidK(1-278)-GFP was a gift from John Rubinstein (Addgene plasmid #184276; pYMA3_SidK_GFP) (Maxson et al., 2022). HeLa cells constitutively expressing V_1A-GFP were generated by amplifying the V_1A-GFP open reading frame using primers 5′-cggaccgATGG ATTTTTCCAAGCTAC-3′ and 5′-ATcggtccgTTACTTGTACAGCTCG-3′ and subcloning via RsrII restriction sites into pRRLSIN. cPPT.PGK-GFP.WPRE. The plasmid used for the generation of pLX307-SopF-V5 was a gift from Leigh Knodler (Addgene plasmid #135174; pmCherry-SopF) (Lau et al., 2019). To generate HeLa cells constitutively expressing SopF-V5, the SopF open reading frame was amplified using primers 5′-gctagcATGCTCAAACCTATCTGCC-3′ and 5′-cccgggATA TAATATTATGCAGTCTCTATT-3′ and subcloned into pJet1.2/blunt. After sequencing, the SopF fragment was cloned into the pLX307 lentiviral vector using restriction sites NheI and SmaI. Virus production and transduction of cells were done as described previously (Agop-Nersesian et al., 2017). The VSV-G envelope expressing plasmid pMD2.G (Addgene plasmid #12259) and the second-generation packaging plasmid psPAX2 (Addgene plasmid #12260) as well as the lentiviral expression plasmid pRRLSIN.cPPT. PGK-GFP.WPRE (Addgene plasmid #12252) were generous gifts from Didier Trono. The lentiviral expression plasmid pLX307 was a gift from William Hahn and Sefi Rosenbluh (Addgene plasmid #98343) (Rosenbluh et al., 2016). For SopF-expressing cells, cells were selected from 2 days after lentiviral transduction with 1 µg/mL Puromycin for 3 days. Single-cell clones were obtained and confirmed by IFA using an anti-V5 antibody. HeLa cells constitutively expressing GFP-LC3B were described before (Agop-Nersesian et al., 2017). HeLa *ATG16L1*$^{-/-}$, *ATG16L1*$^{-/-}$ + BFP-ATG16L1, *ATG16L1*$^{-/-}$ + BFP-ATG16L1-ΔWD40, and GFP-STING1 cells were described before (Fischer et al., 2020). The addbacks are based on the β isoform of ATG16L1. The *STING1*$^{-/-}$ cells were kindly provided by Prof. van Kuppeveld (Utrecht University, Utrecht, The Netherlands) and were generated as described in (Langereis et al., 2015).

4.5 | Generation of HuH7 ATG16L1 knockout cells

For the generation of HuH7 *ATG16L1*$^{-/-}$ cells, the CRISPR/Cas9 GeCKO v2 lentiviral system, described by the Zhang laboratory (Sanjana et al., 2014), was employed. This system comprises two vectors: one encoding for the human-optimized *Streptococcus pyogenes* Cas9 (hSpCas9) enzyme (pLentiCas9-Blast; a gift from Feng Zhang; Addgene #52962; (Sanjana et al., 2014)) and the other containing the single guideRNA (pLentiGuide-Puro; a gift from Feng Zhang; Addgene #52963; (Sanjana et al., 2014)). The guideRNA with the sequence 5′-TCTCGGAGCAACTGAGGCGC-3′ was chosen to target exon 1 of the human ATG16L1 gene. The gRNA was cloned into the plasmid according to the protocol of the Zhang laboratory (Sanjana et al., 2014). Lentiviruses were generated as described previously (Agop-Nersesian et al., 2017). HuH7 cells were transduced with both viruses (guideRNA- and Cas9-encoding) and selected from 2 days after transduction with 1 μg/mL puromycin and 4 μg/mL blasticidin for 3 days. The knockout was confirmed through IFA with an antibody against ATG16L1 (Cell Signaling Technology, #8089). To obtain HuH7 *ATG16L1*$^{-/-}$ clonal cell lines, single cells were grown in 96 well plates and the knockout was confirmed by Western Blot.

4.6 | Transfection of cells

HeLa cells were harvested by accutase treatment, and 1×10^6 cells were pelleted by centrifugation at 700 ***g*** for 3 min at room temperature. Cells were resuspended in Nucleofector V solution (Lonza, VVCA-1003) and transfected with 1 μg of plasmid DNA using program T-028 of the Nucleofector 2b transfection device according to the manufacturer's instructions.

4.7 | Protein lysates and western blotting

Cells were grown in a 6-well plate with 80% confluency. The medium was removed, and cells were rinsed with PBS and lysed directly in the well with 200 μL Laemmli sample buffer (2% glycerol, 25 mM Tris HCl pH 6.8, 0.8% SDS, 0.004% bromophenolblue, 2% 2-mercaptoethanol) preheated to 95°C. Next, the lysate was transferred to an Eppendorf tube and treated with universal nuclease (Thermo Fisher Scientific, 88701) for 5 min at room temperature. Proteins were denatured at 95°C for 5 min. To detect ATG16L1, the proteins were separated on 12% SDS PAGE. PageRuler Prestained NIR Protein Ladder (Thermo Fisher Scientific, 26635) was used as a molecular weight marker. The transfer to nitrocellulose membranes was performed in a tank blot device (Hoefer). Five percent fat-free milk in TBS (Tris-buffered saline; 10 mM Tris, 150 mM NaCl) was used for blocking the membrane. Antibodies were diluted in 3% BSA/PBS. Antibodies used were rabbit mAB anti-ATG16L1 (Cell Signaling Technology, #8089, 1:500) and mouse anti-α-tubulin (Sigma-Aldrich, T6199, 1:1000). For secondary antibody incubation, anti-rabbit IgG 800 CW IRDye and anti-mouse IgG 680 LT IRDye (Li-Cor Biosciences, all 1:10,000) were used. A Li-Cor Odyssey Imaging system (Li-Cor Biosciences) was used for detection.

4.8 | Indirect immunofluorescence analysis

After the indicated time, cells grown on glass coverslips were fixed with 4% paraformaldehyde in PBS for 10 min. Subsequently, they were permeabilized in 0.05% Triton X-100 (Fluka Chemie, T8787) in PBS for 5 min. Unspecific binding sites were blocked by incubation in 10% FCS/PBS for 10 min. Cells were then incubated with primary antibody diluted in 10% FCS/PBS for 1 h. After washing with PBS, cells were incubated with fluorescently labeled secondary antibodies 1:1000 in 10% FCS/PBS for 1 h.

For ATG16L1 staining, cells were permeabilized using 0.05% Triton X-100 (Fluka Chemie, T8787) in PBS for 5 min. Blocking was conducted using 5% FCS/PBS containing 0.3% Triton X-100. Both primary and secondary antibodies were diluted in 1% BSA/PBS containing 0.3% Triton X-100.

The primary antibodies used were rabbit anti-UIS4 antiserum (1:5000), rat anti-UIS4 antiserum (1:5000), chicken anti-UIS4 antiserum (1:5000), rabbit monoclonal anti-ATG16L1 antibody (Cell Signaling, #8089; 1:1000), mouse monoclonal anti-V5 antibody (Invitrogen R960-25, 1:1000), mouse monoclonal anti-LC3 antibody (MBL M152-3; 1:1000), mouse monoclonal anti-GFP antibody (Roche 11814460001; 1:1000), and rabbit monoclonal anti-GFP antibody (Cell Signaling, CS2956, 1:1000). Secondary antibodies were anti-chicken Alexa594 (Invitrogen A-11042; 1:1000), anti-rat Alexa594 (Invitrogen A-11007; 1:1000), anti-rabbit Cy5 (Dianova; 1:1000), anti-rabbit Alexa488 (Invitrogen A-11008; 1:1000), anti-rat Alexa647 (Invitrogen A-21247; 1:1000), anti-mouse Alexa488 (Invitrogen A-11001), and anti-mouse Cy5 (Dianova; 1:1000).

All steps were carried out at room temperature. Labeled cells were mounted on microscope slides with ProLong® Gold Antifade mounting medium (Thermo Fisher Scientific, P36930).

4.9 | Microscopy and quantifications

Confocal images were acquired with an inverted Leica TCS SP8 using an HC PL APO CS2 63×/1.4 NA immersion oil objective. Images were deconvolved using Huygens Professional. Mander's overlap coefficient (MOC) was calculated using the Coloc2 tool of the FIJI software. Costes threshold regression method was employed to automatically determine the threshold value for identifying background. Image processing was performed using FIJI. Quantification of ATG16L1-positive or LC3B-positive parasites was done by visual inspection using a Leica DM5500B epifluorescence microscope. Only UIS4-positive parasites were considered. Parasites were counted positive if a clear association between the protein of interest and UIS4 at the parasite circumference was observed which means that more than 30% of the proximity of the parasite was covered with the protein of interest.

Automated live-cell imaging was used to determine parasite size and numbers. Cells were seeded in a 96-well format and infected with mCherry-expressing parasites. The same cells were imaged with an INCell Analyzer 2000 automated live-cell imaging system (GE Healthcare Life Sciences) at 6 hpi, 24 hpi, and 48 hpi with minimal light exposure (15–25 ms). INCell Developer Toolbox 1.10.0 software was used to analyze the acquired images. The mCherry cytoplasmic signal was used to determine the parasite area. Segmentation was done using the "object" mode in the mCherry channel, and post-processing 2 was done to exclude objects smaller than 10 μm^2.

4.10 | Statistical analysis

All experiments were repeated at least three times independently unless otherwise indicated in the legend of the respective figure. The total number of experiments and sample size analyzed are indicated in the respective figure legend. Mean and standard deviations are indicated. All experimental conditions were statistically analyzed by either a 2-tailed, unpaired Student's *t* test when comparing two groups only, or a one-way ANOVA test when comparing multiple conditions. ANOVA tests were coupled to Tukey's post hoc test to analyze pairwise conditions or to Dunnett's test to compare different groups to the same control. GraphPad Prism version 9 was used to perform statistical analysis and draw graphs.

AUTHOR CONTRIBUTIONS

Annina Bindschedler: Conceptualization; investigation; methodology; writing – original draft; writing – review and editing; visualization. **Jacqueline Schmuckli-Maurer:** Conceptualization; investigation; writing – review and editing. **Sophie Buchser:** Investigation; writing – review and editing. **Tara D. Fischer:** Writing – review and editing; resources. **Rahel Wacker:** Investigation. **Tim Davalan:** Investigation. **Jessica Brunner:** Investigation. **Volker T. Heussler:** Writing – original draft; writing – review and editing; supervision; funding acquisition; conceptualization; project administration.

ACKNOWLEDGMENTS

We thank Prof. Dr. Richard Youle for providing the HeLa ATG16L1$^{-/-}$, ATG16L1$^{-/-}$ + BFP-ATG16L1, ATG16L1$^{-/-}$ + BFP-ATG16L1-ΔWD40, and GFP-STING1 cell lines. Prof. Dr. Frank van Kuppeveld is acknowledged for supplying the *STING1*$^{-/-}$ cell line. Dr. Kerry Woods is thanked for critically reading the manuscript. We thank the MIC (Microscopy Imaging Centre) in Bern for providing excellent imaging facilities and technical support. This work was supported by the Intramural Research Program of the National Institute of Neurological Disorders and Stroke (1ZIANS003127-08). This work was funded by the Swiss National Science Foundation (SNSF) (grant number 310030_182465) and an Multidisciplinary Center for Infectious Diseases (MCID), University of Bern, Switzerland grant to Volker Heussler (MA-09). Open access funding provided by Universitat Bern.

CONFLICT OF INTEREST STATEMENT

The authors declare no conflict of interest.

DATA AVAILABILITY STATEMENT

All relevant data are within the paper. The data supporting this study's findings are available on request from the corresponding author.

ETHICS STATEMENT

The study was performed in strict accordance with the guidelines of the Swiss Tierschutzgesetz (TSCHG; Animal Rights Laws) and approved by the ethical commitee of the University of Bern (Permit number: BE98/19).

ORCID

Annina Bindschedler https://orcid.org/0000-0003-0336-0864

REFERENCES

Abbas, Y.M., Wu, D., Bueler, S.A., Robinson, C.V. & Rubinstein, J.L. (2020) Structure of V-ATPase from the mammalian brain. *Science*, 367(6483), 1240–1246. Available from: https://doi.org/10.1126/science.aaz2924

Afriat, A., Zuzarte-Luis, V., Bahar Halpern, K., Buchauer, L., Marques, S., Chora, A.F. et al. (2022) A spatiotemporally resolved single-cell atlas of the *Plasmodium* liver stage. *Nature*, 611(7936), 563–569. Available from: https://doi.org/10.1038/s41586-022-05406-5

Agop-Nersesian, C., De Niz, M., Niklaus, L., Prado, M., Eickel, N. & Heussler, V.T. (2017) Shedding of host autophagic proteins from the parasitophorous vacuolar membrane of *Plasmodium berghei*. *Scientific Reports*, 7(1), 2191. Available from: https://doi.org/10.1038/s41598-017-02156-7

Agop-Nersesian, C., Niklaus, L., Wacker, R. & Heussler, V.T. (2018) Host cell cytosolic immune response during *Plasmodium* liver stage development. *FEMS Microbiology Reviews*, 42(3), 324–334. Available from: https://doi.org/10.1093/femsre/fuy007

Aguilera, M.O., Delgui, L.R., Reggiori, F., Romano, P.S. & Colombo, M.I. (2024) Autophagy as an innate immunity response against pathogens: a Tango dance. *FEBS Letters*, 598(1), 140–166. Available from: https://doi.org/10.1002/1873-3468.14788

Ahn, J. & Barber, G.N. (2019) STING signaling and host defense against microbial infection. *Experimental & Molecular Medicine*, 51(12), 1–10. Available from: https://doi.org/10.1038/s12276-019-0333-0

Amino, R., Giovannini, D., Thiberge, S., Gueirard, P., Boisson, B., Dubremetz, J.F. et al. (2008) Host cell traversal is important for progression of the malaria parasite through the dermis to the liver. *Cell Host & Microbe*, 3(2), 88–96. Available from: https://doi.org/10.1016/j.chom.2007.12.007

Amino, R., Thiberge, S., Martin, B., Celli, S., Shorte, S., Frischknecht, F. et al. (2006) Quantitative imaging of *Plasmodium* transmission from mosquito to mammal. *Nature Medicine*, 12(2), 220–224. Available from: https://doi.org/10.1038/nm1350

Bano, N., Romano, J.D., Jayabalasingham, B. & Coppens, I. (2007) Cellular interactions of *Plasmodium* liver stage with its host mammalian cell. *International Journal for Parasitology*, 37(12), 1329–1341. Available from: https://doi.org/10.1016/j.ijpara.2007.04.005

Bindschedler, A., Schmuckli-Maurer, J., Wacker, R., Kramer, N., Rehmann, R., Caldelari, R. et al. (2022) *Plasmodium berghei*-mediated NRF2 activation in infected hepatocytes enhances parasite survival. *Cellular Microbiology*, 2022, 7647976. Available from: https://doi.org/10.1155/2022/7647976

Bindschedler, A., Wacker, R., Egli, J., Eickel, N., Schmuckli-Maurer, J., Franke-Fayard, B.M. et al. (2021) *Plasmodium berghei* sporozoites in nonreplicative vacuoles are eliminated by a PI3P-mediated autophagy-independent pathway. *Cellular Microbiology*, 23(1), e13271. Available from: https://doi.org/10.1111/cmi.13271

Boonhok, R., Rachaphaew, N., Duangmanee, A., Chobson, P., Pattaradilokrat, S., Utaisincharoen, P. et al. (2016) LAP-like process as an immune mechanism downstream of IFN-gamma in control of the human malaria *Plasmodium vivax* liver stage. *Proceedings of the National Academy of Sciences of the United States of America*, 113(25), E3519–E3528. Available from: https://doi.org/10.1073/pnas.1525606113

Burda, P.C., Roelli, M.A., Schaffner, M., Khan, S.M., Janse, C.J. & Heussler, V.T. (2015) A *Plasmodium* phospholipase is involved in disruption of the liver stage parasitophorous vacuole membrane. *PLoS Pathogens*, 11(3), e1004760. Available from: https://doi.org/10.1371/journal.ppat.1004760

Burdette, D.L. & Vance, R.E. (2013) STING and the innate immune response to nucleic acids in the cytosol. *Nature Immunology*, 14(1), 19–26. Available from: https://doi.org/10.1038/ni.2491

Chen, Q., Sun, L. & Chen, Z.J. (2016) Regulation and function of the cGAS-STING pathway of cytosolic DNA sensing. *Nature Immunology*, 17(10), 1142–1149. Available from: https://doi.org/10.1038/ni.3558

Collins, M.P. & Forgac, M. (2020) Regulation and function of V-ATPases in physiology and disease. *Biochimica et Biophysica Acta - Biomembranes*, 1862(12), 183341. Available from: https://doi.org/10.1016/j.bbamem.2020.183341

Dhanwani, R., Takahashi, M. & Sharma, S. (2018) Cytosolic sensing of immuno-stimulatory DNA, the enemy within. *Current Opinion in Immunology*, 50, 82–87. Available from: https://doi.org/10.1016/j.coi.2017.11.004

Dooley, H.C., Razi, M., Polson, H.E., Girardin, S.E., Wilson, M.I. & Tooze, S.A. (2014) WIPI2 links LC3 conjugation with PI3P, autophagosome formation, and pathogen clearance by recruiting Atg12-5-16L1. *Molecular Cell*, 55(2), 238–252. Available from: https://doi.org/10.1016/j.molcel.2014.05.021

Durgan, J. & Florey, O. (2022) Many roads lead to CASM: diverse stimuli of noncanonical autophagy share a unifying molecular mechanism. *Science Advances*, 8(43), eabo1274. Available from: https://doi.org/10.1126/sciadv.abo1274

Durgan, J., Lystad, A.H., Sloan, K., Carlsson, S.R., Wilson, M.I., Marcassa, E. et al. (2021) Non-canonical autophagy drives alternative ATG8 conjugation to phosphatidylserine. *Molecular Cell*, 81(9), 2031–2040 e2038. Available from: https://doi.org/10.1016/j.molcel.2021.03.020

Fischer, T.D., Wang, C., Padman, B.S., Lazarou, M. & Youle, R.J. (2020) STING induces LC3B lipidation onto single-membrane vesicles via the V-ATPase and ATG16L1-WD40 domain. *The Journal of Cell Biology*, 219(12). Available from: https://doi.org/10.1083/jcb.202009128

Fletcher, K., Ulferts, R., Jacquin, E., Veith, T., Gammoh, N., Arasteh, J.M. et al. (2018) The WD40 domain of ATG16L1 is required for its non-canonical role in lipidation of LC3 at single membranes. *The EMBO Journal*, 37(4). Available from: https://doi.org/10.15252/embj.201797840

Florey, O., Gammoh, N., Kim, S.E., Jiang, X. & Overholtzer, M. (2015) V-ATPase and osmotic imbalances activate endolysosomal LC3 lipidation. *Autophagy*, 11(1), 88–99. Available from: https://doi.org/10.4161/15548627.2014.984277

Florey, O., Kim, S.E., Sandoval, C.P., Haynes, C.M. & Overholtzer, M. (2011) Autophagy machinery mediates macroendocytic processing and entotic cell death by targeting single membranes. *Nature Cell Biology*, 13(11), 1335–1343. Available from: https://doi.org/10.1038/ncb2363

Florey, O. & Overholtzer, M. (2012) Autophagy proteins in macroendocytic engulfment. *Trends in Cell Biology*, 22(7), 374–380. Available from: https://doi.org/10.1016/j.tcb.2012.04.005

Frischknecht, F., Baldacci, P., Martin, B., Zimmer, C., Thiberge, S., Olivo-Marin, J.C. et al. (2004) Imaging movement of malaria parasites during transmission by anopheles mosquitoes. *Cellular Microbiology*, 6(7), 687–694. Available from: https://doi.org/10.1111/j.1462-5822.2004.00395.x

Gammoh, N., Florey, O., Overholtzer, M. & Jiang, X. (2013) Interaction between FIP200 and ATG16L1 distinguishes ULK1 complex-dependent and -independent autophagy. *Nature Structural & Molecular Biology*, 20(2), 144–149. Available from: https://doi.org/10.1038/nsmb.2475

Grützke, J., Rindte, K., Goosmann, C., Silvie, O., Rauch, C., Heuer, D. et al. (2014) The spatiotemporal dynamics and membranous features of the *Plasmodium* liver stage tubovesicular network. *Traffic*, 15(4), 362–382. Available from: https://doi.org/10.1111/tra.12151

Gui, X., Yang, H., Li, T., Tan, X., Shi, P., Li, M. et al. (2019) Autophagy induction via STING trafficking is a primordial function of the cGAS pathway. *Nature*, 567(7747), 262–266. Available from: https://doi.org/10.1038/s41586-019-1006-9

Hayashi, M., Yamada, H., Mitamura, T., Horii, T., Yamamoto, A. & Moriyama, Y. (2000) Vacuolar H(+)-ATPase localized in plasma membranes of malaria parasite cells, *Plasmodium falciparum*, is involved in regional acidification of parasitized erythrocytes. *The Journal of Biological Chemistry*, 275(44), 34353–34358. Available from: https://doi.org/10.1074/jbc.M003323200

Heckmann, B.L. & Green, D.R. (2019) LC3-associated phagocytosis at a glance. *Journal of Cell Science*, 132(5). Available from: https://doi.org/10.1242/jcs.222984

Hooper, K.M., Jacquin, E., Li, T., Goodwin, J.M., Brumell, J.H., Durgan, J. et al. (2022) V-ATPase is a universal regulator of LC3-associated phagocytosis and non-canonical autophagy. *The Journal of Cell Biology*, 221(6). Available from: https://doi.org/10.1083/jcb.202105112

Ichimura, Y., Kirisako, T., Takao, T., Satomi, Y., Shimonishi, Y., Ishihara, N. et al. (2000) A ubiquitin-like system mediates protein lipidation. *Nature*, 408(6811), 488–492. Available from: https://doi.org/10.1038/35044114

Jacquin, E., Leclerc-Mercier, S., Judon, C., Blanchard, E., Fraitag, S. & Florey, O. (2017) Pharmacological modulators of autophagy activate a parallel noncanonical pathway driving unconventional LC3 lipidation. *Autophagy*, 13(5), 854–867. Available from: https://doi.org/10.1080/15548627.2017.1287653

Kabeya, Y., Mizushima, N., Ueno, T., Yamamoto, A., Kirisako, T., Noda, T. et al. (2000) LC3, a mammalian homologue of yeast Apg8p, is localized in autophagosome membranes after processing. *The EMBO Journal*, 19(21), 5720–5728. Available from: https://doi.org/10.1093/emboj/19.21.5720

Langereis, M.A., Rabouw, H.H., Holwerda, M., Visser, L.J. & van Kuppeveld, F.J. (2015) Knockout of cGAS and STING rescues virus infection of plasmid DNA-transfected cells. *Journal of Virology*, 89(21), 11169–11173. Available from: https://doi.org/10.1128/JVI.01781-15

Lau, N., Haeberle, A.L., O'Keeffe, B.J., Latomanski, E.A., Celli, J., Newton, H.J. et al. (2019) SopF, a phosphoinositide binding effector, promotes the stability of the nascent Salmonella-containing vacuole. *PLoS Pathogens*, 15(7), e1007959. Available from: https://doi.org/10.1371/journal.ppat.1007959

Levine, B., Mizushima, N. & Virgin, H.W. (2011) Autophagy in immunity and inflammation. *Nature*, 469(7330), 323–335. Available from: https://doi.org/10.1038/nature09782

Lystad, A.H., Carlsson, S.R., de la Ballina, L.R., Kauffman, K.J., Nag, S., Yoshimori, T. et al. (2019) Distinct functions of ATG16L1 isoforms in membrane binding and LC3B lipidation in autophagy-related

processes. *Nature Cell Biology*, 21(3), 372–383. Available from: https://doi.org/10.1038/s41556-019-0274-9

Marques-da-Silva, C., Poudel, B., Baptista, R.P., Peissig, K., Hancox, L.S., Shiau, J.C. et al. (2023) AIM2 sensors mediate immunity to *Plasmodium* infection in hepatocytes. *Proceedings of the National Academy of Sciences of the United States of America*, 120(2), e2210181120. Available from: https://doi.org/10.1073/pnas.2210181120

Martinez, J., Malireddi, R.K., Lu, Q., Cunha, L.D., Pelletier, S., Gingras, S. et al. (2015) Molecular characterization of LC3-associated phagocytosis reveals distinct roles for Rubicon, NOX2 and autophagy proteins. *Nature Cell Biology*, 17(7), 893–906. Available from: https://doi.org/10.1038/ncb3192

Maxson, M.E., Abbas, Y.M., Wu, J.Z., Plumb, J.D., Grinstein, S. & Rubinstein, J.L. (2022) Detection and quantification of the vacuolar H+ATPase using the legionella effector protein SidK. *The Journal of Cell Biology*, 221(3). Available from: https://doi.org/10.1083/jcb.202107174

Melia, T.J., Lystad, A.H. & Simonsen, A. (2020) Autophagosome biogenesis: from membrane growth to closure. *The Journal of Cell Biology*, 219(6). Available from: https://doi.org/10.1083/jcb.202002085

Mizushima, N. (2010) The role of the Atg1/ULK1 complex in autophagy regulation. *Current Opinion in Cell Biology*, 22(2), 132–139. Available from: https://doi.org/10.1016/j.ceb.2009.12.004

Morishita, H. & Mizushima, N. (2019) Diverse cellular roles of autophagy. *Annual Review of Cell and Developmental Biology*, 35, 453–475. Available from: https://doi.org/10.1146/annurev-cellbio-100818-125300

Nakatogawa, H. (2013) Two ubiquitin-like conjugation systems that mediate membrane formation during autophagy. *Essays in Biochemistry*, 55, 39–50. Available from: https://doi.org/10.1042/bse0550039

Niklaus, L., Agop-Nersesian, C., Schmuckli-Maurer, J., Wacker, R., Grunig, V. & Heussler, V.T. (2019) Deciphering host lysosome-mediated elimination of *Plasmodium berghei* liver stage parasites. *Scientific Reports*, 9(1), 7967. Available from: https://doi.org/10.1038/s41598-019-44449-z

Ohkuma, S., Moriyama, Y. & Takano, T. (1982) Identification and characterization of a proton pump on lysosomes by fluorescein-isothiocyanate-dextran fluorescence. *Proceedings of the National Academy of Sciences of the United States of America*, 79(9), 2758–2762. Available from: https://doi.org/10.1073/pnas.79.9.2758

Pradel, G. & Frevert, U. (2001) Malaria sporozoites actively enter and pass through rat Kupffer cells prior to hepatocyte invasion. *Hepatology*, 33(5), 1154–1165. Available from: https://doi.org/10.1053/jhep.2001.24237

Prado, M., Eickel, N., De Niz, M., Heitmann, A., Agop-Nersesian, C., Wacker, R. et al. (2015) Long-term live imaging reveals cytosolic immune responses of host hepatocytes against *Plasmodium* infection and parasite escape mechanisms. *Autophagy*, 11(9), 1561–1579. Available from: https://doi.org/10.1080/15548627.2015.1067361

Real, E., Rodrigues, L., Cabal, G.G., Enguita, F.J., Mancio-Silva, L., Mello-Vieira, J. et al. (2018) *Plasmodium* UIS3 sequesters host LC3 to avoid elimination by autophagy in hepatocytes. *Nature Microbiology*, 3(1), 17–25. Available from: https://doi.org/10.1038/s41564-017-0054-x

Romano, P.S., Akematsu, T., Besteiro, S., Bindschedler, A., Carruthers, V.B., Chahine, Z. et al. (2023) Autophagy in protists and their hosts: when, how and why? *Autophagy Reports*, 2(1), 2149211. Available from: https://doi.org/10.1080/27694127.2022.2149211

Rosenbluh, J., Mercer, J., Shrestha, Y., Oliver, R., Tamayo, P., Doench, J.G. et al. (2016) Genetic and proteomic interrogation of lower confidence candidate genes reveals signaling networks in beta-catenin-active cancers. *Cell Systems*, 3(3), 302–316 e304. Available from: https://doi.org/10.1016/j.cels.2016.09.001

Russell, R.C., Tian, Y., Yuan, H., Park, H.W., Chang, Y.Y., Kim, J. et al. (2013) ULK1 induces autophagy by phosphorylating Beclin-1 and activating VPS34 lipid kinase. *Nature Cell Biology*, 15(7), 741–750. Available from: https://doi.org/10.1038/ncb2757

Sanjana, N.E., Shalem, O. & Zhang, F. (2014) Improved vectors and genome-wide libraries for CRISPR screening. *Nature Methods*, 11(8), 783–784. Available from: https://doi.org/10.1038/nmeth.3047

Schmuckli-Maurer, J., Reber, V., Wacker, R., Bindschedler, A., Zakher, A. & Heussler, V.T. (2017) Inverted recruitment of autophagy proteins to the *Plasmodium berghei* parasitophorous vacuole membrane. *PLoS One*, 12(8), e0183797. Available from: https://doi.org/10.1371/journal.pone.0183797

Setua, S., Enguita, F.J., Chora, A.F., Ranga-Prasad, H., Lahree, A., Marques, S. et al. (2020) Disrupting *Plasmodium* UIS3-host LC3 interaction with a small molecule causes parasite elimination from host cells. *Communications Biology*, 3(1), 688. Available from: https://doi.org/10.1038/s42003-020-01422-1

Spielmann, T., Montagna, G.N., Hecht, L. & Matuschewski, K. (2012) Molecular make-up of the *Plasmodium* parasitophorous vacuolar membrane. *International Journal of Medical Microbiology*, 302(4–5), 179–186. Available from: https://doi.org/10.1016/j.ijmm.2012.07.011

Stewart, A.G., Sobti, M., Harvey, R.P. & Stock, D. (2013) Rotary ATPases: models, machine elements and technical specifications. *BioArchitecture*, 3(1), 2–12. Available from: https://doi.org/10.4161/bioa.23301

Sturm, A., Amino, R., van de Sand, C., Regen, T., Retzlaff, S., Rennenberg, A. et al. (2006) Manipulation of host hepatocytes by the malaria parasite for delivery into liver sinusoids. *Science*, 313(5791), 1287–1290. Available from: https://doi.org/10.1126/science.1129720

Tavares, J., Formaglio, P., Thiberge, S., Mordelet, E., Van Rooijen, N., Medvinsky, A. et al. (2013) Role of host cell traversal by the malaria sporozoite during liver infection. *The Journal of Experimental Medicine*, 210(5), 905–915. Available from: https://doi.org/10.1084/jem.20121130

Thieleke-Matos, C., Lopes da Silva, M., Cabrita-Santos, L., Portal, M.D., Rodrigues, I.P., Zuzarte-Luis, V. et al. (2016) Host cell autophagy contributes to *Plasmodium* liver development. *Cellular Microbiology*, 18(3), 437–450. Available from: https://doi.org/10.1111/cmi.12524

van Schalkwyk, D.A., Chan, X.W., Misiano, P., Gagliardi, S., Farina, C. & Saliba, K.J. (2010) Inhibition of *Plasmodium falciparum* pH regulation by small molecule indole derivatives results in rapid parasite death. *Biochemical Pharmacology*, 79(9), 1291–1299. Available from: https://doi.org/10.1016/j.bcp.2009.12.025

Wacker, R., Eickel, N., Schmuckli-Maurer, J., Annoura, T., Niklaus, L., Khan, S.M. et al. (2017) LC3-association with the parasitophorous vacuole membrane of *Plasmodium berghei* liver stages follows a noncanonical autophagy pathway. *Cellular Microbiology*, 19(10). Available from: https://doi.org/10.1111/cmi.12754

WHO. (2022) World Malaria Report 2022. (ISBN 978-92-4-006489-8).

Xu, L., Shen, X., Bryan, A., Banga, S., Swanson, M.S. & Luo, Z.Q. (2010) Inhibition of host vacuolar H+-ATPase activity by a Legionella pneumophila effector. *PLoS Pathogens*, 6(3), e1000822. Available from: https://doi.org/10.1371/journal.ppat.1000822

Xu, Y., Zhou, P., Cheng, S., Lu, Q., Nowak, K., Hopp, A.K. et al. (2019) A bacterial effector reveals the V-ATPase-ATG16L1 Axis that initiates Xenophagy. *Cell*, 178(3), 552–566 e520. Available from: https://doi.org/10.1016/j.cell.2019.06.007

Yang, Z. & Klionsky, D.J. (2010) Mammalian autophagy: core molecular machinery and signaling regulation. *Current Opinion in Cell Biology*, 22(2), 124–131. Available from: https://doi.org/10.1016/j.ceb.2009.11.014

Yeung, T., Gilbert, G.E., Shi, J., Silvius, J., Kapus, A. & Grinstein, S. (2008) Membrane phosphatidylserine regulates surface charge and protein localization. *Science*, 319(5860), 210–213. Available from: https://doi.org/10.1126/science.1152066

Yoshimori, T., Yamamoto, A., Moriyama, Y., Futai, M. & Tashiro, Y. (1991) Bafilomycin A1, a specific inhibitor of vacuolar-type H(+)-ATPase, inhibits acidification and protein degradation in lysosomes of cultured cells. *The Journal of Biological Chemistry*, 266(26), 17707–17712.

Zhang, C.S., Jiang, B., Li, M., Zhu, M., Peng, Y., Zhang, Y.L. et al. (2014) The lysosomal v-ATPase-Ragulator complex is a common activator for AMPK and mTORC1, acting as a switch between catabolism and anabolism. *Cell Metabolism*, 20(3), 526–540. Available from: https://doi.org/10.1016/j.cmet.2014.06.014

Zhao, C., Liu, T., Zhou, T., Fu, Y., Zheng, H., Ding, Y. et al. (2016) The rodent malaria liver stage survives in the rapamycin-induced autophagosome of infected Hepa1-6 cells. *Scientific Reports*, 6, 38170. Available from: https://doi.org/10.1038/srep38170

Zhao, J., Beyrakhova, K., Liu, Y., Alvarez, C.P., Bueler, S.A., Xu, L. et al. (2017) Molecular basis for the binding and modulation of V-ATPase by a bacterial effector protein. *PLoS Pathogens*, 13(6), e1006394. Available from: https://doi.org/10.1371/journal.ppat.1006394

Zoncu, R., Bar-Peled, L., Efeyan, A., Wang, S., Sancak, Y. & Sabatini, D.M. (2011) mTORC1 senses lysosomal amino acids through an inside-out mechanism that requires the vacuolar H(+)-ATPase. *Science*, 334(6056), 678–683. Available from: https://doi.org/10.1126/science.1207056

SUPPORTING INFORMATION

Additional supporting information can be found online in the Supporting Information section at the end of this article.

How to cite this article: Bindschedler, A., Schmuckli-Maurer, J., Buchser, S., Fischer, T.D., Wacker, R., Davalan, T. et al. (2024) LC3B labeling of the parasitophorous vacuole membrane of *Plasmodium berghei* liver stage parasites depends on the V-ATPase and ATG16L1. *Molecular Microbiology*, 00, 1–17. Available from: https://doi.org/10.1111/mmi.15259